Utrecht University

Faculteit Bètawetenschappen

Multiplicity dependence of particle production in pp collisions with PYTHIA

Bachelor Thesis

Bas Hofman

Physics and Astronomy

Supervisor:

Dr. Panos Christakoglou
Institute for Subatomic Physics at Utrecht University
Dutch National Institute for Subatomic Physics (NIKHEF)

June 13, 2018

Abstract

In this thesis we compare the transverse momentum of specific particle species for PYTHIA datasets in pp events with a center of mass energy of 7 TeV. We compare the results for a PYTHIA dataset where the colour reconnection (CR) mechanism is switched on and a PYTHIA dataset where the CR mechanism is switched off. The overall mean p_{T} for events CR events is significantly higher than for no CR events. The effects of CR seems to be more prominent in heavier particles. The data seems to suggest a linear mass dependence for the increase in p_{T}.

Contents

Part I. Summary

The field of heavy-ion physics focuses on the study and characterization of the Quark Gluon Plasma (QGP). The QGP is a form of matter that is believed to have existed a few fractions of a second after the big bang. In this state of matter quarks can behave as quasi-free particles and the plasma behaves as a super fluid. It is generally believed this state of matter is created during heavy ion collisions at the LHC and RHIC accelerators. Recent results have suggested that this form of matter may also be created in smaller systems like pp and p-Pb. Whether or not a QGP is formed in these systems is still an ongoing debate and therefore these systems are an interesting research topic. This thesis will focus on such a system, namely the pp system.

This thesis will be a study on particle production using the PYTHIA model. We will be analyzing two different PYTHIA datasets for pp events at a center of mass energy of 7 TeV, the difference being the mechanism of colour reconnection. One dataset will include a colour reconnection mechanism while the other dataset will have no form of colour reconnection whatsoever. For these datasets we analyze three η ranges, namely $|\eta| \leq 0.8$, which is the acceptance of ALICE, $|\eta| \leq 1.6$ and $|\eta| \leq 2.4$, which is the acceptance of CMS. In particular we will focus on the transverse momentum of the primary particles created in the events.

Our results show a clear influence of the colour reconnection mechanism on the transverse momentum. The overall mean transverse momentum for events with colour reconnection is significantly higher than for particles without colour reconnection. When we also take multiplicity into account we see that for low multiplicity events the mean transverse momentum for colour reconnected events is actually slightly lower in comparison to the non colour reconnected dataset. This effect is however overshadowed by the significant boost in transverse momentum for particles in high multiplicity events. The effects of the colour reconnection mechanism on the transverse momentum seems to be more prominent in heavier particles. The results in this thesis seem to suggest a linear mass dependence for the increase in transverse momentum and are in qualitative agreement with experimental measurements.

Part II. Theory

1 The Standard Model of Particle Physics

In particle physics the Standard Model is a model describing the interactions between fundamental particles that make up matter as we know it and the forces acting on them. Three out of the four forces of nature are included in the Standard Model, the electromagnetic, the weak and the strong force. Gravitational force is not part of the Standard Model.

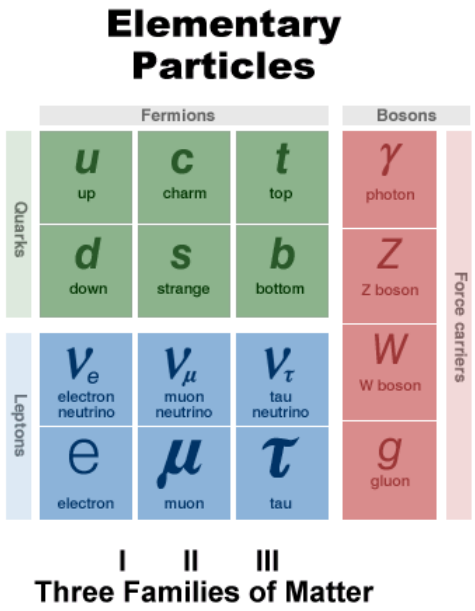

Fig. 1: The Standard Model of particle physics

Fundamental particles are particles that are believed to have no substructure, meaning they themselves are not composed of particles. The first type of fundamental particles are the quarks. There are six quark flavours which are accompanied by their corresponding antiquarks. The quarks can pair up to form baryons, who in turn make up 'ordinary' matter, and mesons.

The second type of fundamental particles are the leptons. They also consist of six particles and their six corresponding antiparticles. The electron is part of this class of particles. The quark and lepton classes constitute the particle class called fermions.

The third type of fundamental particles are the bosons. They play a crucial part in the interactions between the fermions as these bosons are the force carriers of their corresponding force. The force carrier boson for the electromagnetic force is the photon. The weak force is propagated by W and Z bosons, and the force carriers for the strong force are the gluons.

2 Particle accelerators

The discovery of the aforementioned particles and the study of their properties has been facilitated by the usage of particle accelerators. In this form of experiment particles are accelerated up to high energy and then brought into collision with each other inside of a detector. The particles that are propagated out of such an event then can be detected by the detector.

There are particle accelerators on a broad range of sizes and an important variable is the center of mass energy, which is commonly denoted as $\sqrt{s}$. The range of $\sqrt{s}$ goes from a few MeV at small accelerators up to a few TeV at the biggest accelerator. The most energetic particle accelerator to date is the LHC, at CERN, the European Organization for Nuclear Research. The LHC can reach center of mass energies of up to 13 TeV for proton proton collisions. The accelerator complex has a beam pipe with a circumference of 27 kilometers that is fitted with powerful superconducting magnets to steer the particles around. The LHC experiment consists of six different detectors, each consisting of many subdetectors.

There are four main experiments currently conducted at the LHC. They are ALICE, Atlas, CMS and LHCb. The Atlas experiment is doing research on the Higgs particle, CP violation and doing more precise measurements on the top quark. The CMS experiment is a general purpose detector that is also used for the detection of Higgs particles. CMS also is involved in heavy ion physics. LHCb is a detector that is used for specialized beauty physics. This includes research on CP violation. ALICE is the detector that is used primarily for heavy ion physics. One of the phenomena that is studied in ALICE is the Quark-Gluon Plasma. This thesis will be focused on studies related to ALICE.

3 Quark-Gluon Plasma

One of the main pillars of research at the ALICE experiment is the research on a state of matter known as the Quark-Gluon Plasma. The QGP is a form of matter that is believed to have existed a few fractions of a second after the big bang. In this state of matter quarks can behave as quasi-free particles and the plasma behaves as a super fluid. Quarks are generally bound together by the strong force in a process described by colour confinement. In this process the attraction between quarks scales with the distance between them, effectively prohibiting the isolation of these particles. However at sufficiently high temperature and density the interaction between quarks decreases asymptoticly as the energy increases, at which point the QGP forms. It is generally believed this state of matter is created during heavy ion collisions at the LHC and RHIC accelerators. This creates a tool to probe into this interesting form of matter and possibly gives us a look into the past.

4 Particle collisions

To reproduce the state of matter where quarks and gluons are deconfined we use heavy-ion collisions. To disentangle effects that are not related to the quark-gluon plasma from our observations we use reference systems such as pp and p-Pb systems. Until recently is was believed that such systems did not create the needed conditions for the creation of a quark-gluon plasma. However, lately there have been experimental results that in both pp and p-Pb collisions that seem to indicate that such a state of matter can in fact also be created in such small systems. This greatly raises the importance of detailed study of these systems for the field of heavy ion physics. Therefore this thesis will focus on such a system, namely the pp system. In this thesis we will study the effects of colour reconnection on the transverse momentum spectra for specific particles. We will do so by analyzing two datasets generated by the PYTHIA model.

Proton proton collisions are characterized by having a low multiplicity, meaning a low number of particles are created during the event. Collisions between proton beams are also an important tool for the research in perturbative quantum chromodynamics.[3] This type of events also played a big role in the discovery of the Higgs boson.

The other two types of particle collision, the ion proton and ion ion collisions, are commonly referred to as pA and AA respectively. These type of events are characterized by a significantly bigger multiplicity, up orders of magnitude from a typical pp event. Generally these events are also achieved with lower center of mass energies. These two events, known as heavy ion collisions, also play an important role in the research in QCD.

Part III. ALICE

ALICE is an abbreviation for A Large Ion Collider Experiment. The ALICE detector consists of 18 subdetectors[2], each of which is optimized for a specific use. ALICE allows the study of hadrons, electrons, muons and photons. ALICE is a general purpose detector that can measure a broad range of observables that where previously studied by specialized detectors.

During a typical heavy ion collision an extremely high particle multiplicity is created which could be up to 3 order of magnitude higher that during a pp interaction. ALICE is optimized for detecting as much as 4000 charged particles created in a Pb-Pb collision spanning a broad range of momenta. The range in which ALICE is able to observe goes from the scale of a few MeV/c for low momentum particles up to 100 GeV/c for detecting particle jets. This broad momentum range is essential as particle identification (PID) often depends on mass or quark flavour observables. In order to identify particles ALICE utilizes basically all known PID techniques.

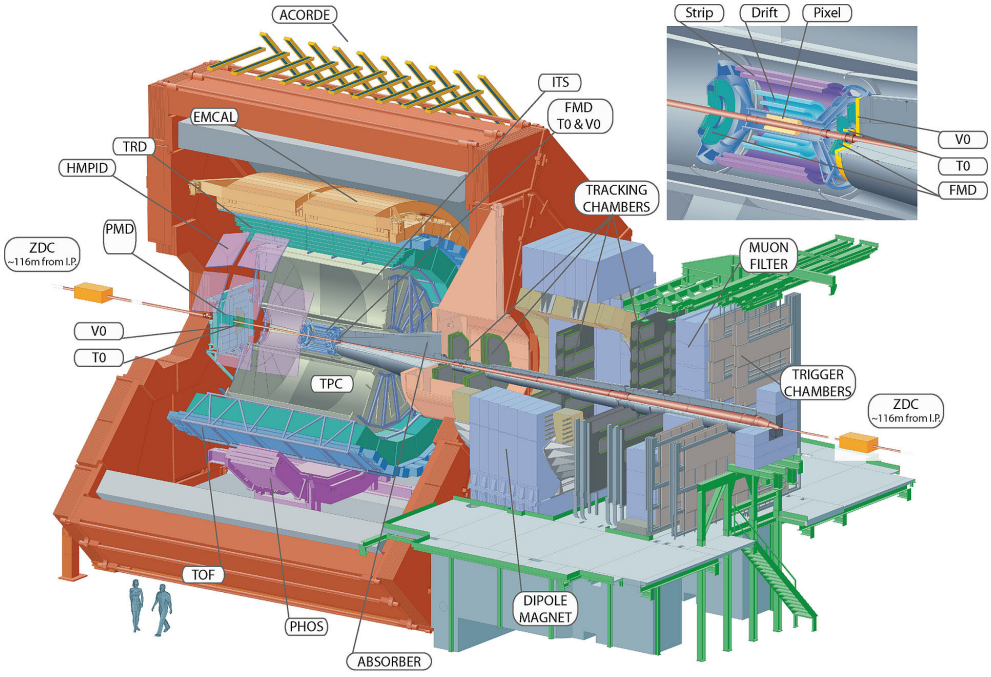

Fig. 2: Cut-away of the ALICE detector showings its subdetectors.

5 Detector layout

The tracking systems in the central barrel are made up of the Inner Tracking Device (ITS), which consists of 6 layers of silicon vertex detectors, and the Time-Projection Chamber (TPC). The TPC has a pseudorapidity coverage of $|\eta| \leq 0.9$

The detector is also equipped with a sophisticated Time of Flight (TOF) array which consists of 160,000 individual cells. For detecting photons ALICE uses a PHOS electromagnetic calorimeter, which is located far from the vertex. For measuring jet properties ALICE is also equipped with a second electromagnetic calorimeter called EMCal.

For the measurement of heavy quark resonances ALICE uses a Muon spectrometer.

Small and specialized detectors are used for triggering and to measure global event characteristics. The event time is measured by the T0 detector. The V0 detector is used as minimum bias trigger. The Forward Multiplicity Detector (FMD) provides information about the multiplicity of charged particles and the Photon Multiplicity Detector (PMD) about the multiplicity and spatial distribution of photons on an event by event basis.

The hardware trigger of ALICE consists of multiple levels to accommodate for the different timing requirements of the detectors. The software based High-Level Trigger (HLT), which is a PC farm, selects and compresses relevant event information.

Part IV. Analysis

The analysis was performed on simulated datasets. The datasets analyzed were created with PYTHIA which is a Monte Carlo generator commonly used to describe pp collisions. In this analysis we used two PYTHIA datasets. One dataset with he inclusion of colour reconnection (CR) which contains 8.4×10^7 events and one dataset without the inclusion of colour reconnection (No CR) which contains 7.2×10^7 events. The type of events simulated are pp events events at a center of mass energy of 7 TeV. The particles analyzed are primary particles that are created in the event. The particles included in this analysis are $\pi^{\pm}$, $p(\bar{p})$, $K^{\pm}$, K^0_s, Λ, Ξ^0, $\Xi^{\pm}$ and Ω^-. For this analysis the ROOT framework created by CERN was used. The two datasets were analysed for three different η cuts. The η cuts included in this analysis are $|\eta| \leq 0.8$, which is the acceptance of ALICE, $|\eta| \leq 1.6$ and $|\eta| \leq 2.4$, which is the acceptance of CMS.

Particle	pdg code	Mass in MeV	Relative mass to proton
$\pi^{\pm}$	211	139.57	0.14
$K^{\pm}$	321	493.67	0.52
K^0_s	310	497.61	0.53
$p(\bar{p})$	2212	938.27	1
Λ	3122	1115.68	1.18
Ξ^0	3322	1314.86	1.40
$\Xi^{\pm}$	3312	1321.71	1.40
Ω^-	3334	1672.45	1.78

Tab. 1: Particle mass[4] of particles used in this analysis

6 Multiplicity binning

The events in this analysis are binned by multiplicity. The multiplicity of an event is the number of primary particles created during the event.

This is done in 10 bins each consisting of roughly 10% of the events. This mean that the 10% highest multiplicity events are binned together in the first bin. The second bin is then filled with the 10% to 20% highest multiplicity events all the way up to the last bin that is filled with the 10% lowest multiplicity events. Figure 3 shows the binning of the multiplicity spectrum and table 2 shows the multiplicity values for each bin used in the analysis.

Multiplicity		$\|\eta\| \leq 0.8$		$\|\eta\| \leq 1.6$		$\|\eta\| \leq 2.4$	
%	bin	CR	No CR	CR	No CR	CR	No CR
90-100%	10	3	3	5	5	7	7
80-90%	9	4	4	7	7	10	10
70-80%	8	5	5	9	10	13	13
60-70%	7	6	7	12	13	16	17
50-60%	6	8	10	15	18	21	24
40-50%	5	10	13	20	25	28	36
30-40%	4	14	18	27	35	38	51
20-30%	3	18	26	36	49	52	75
10-20%	2	25	38	50	70	72	111
0-10%	1	25+	38+	50+	70+	72+	111+

Tab. 2: Multiplicity ranges contained in the classes for varying η range. The table shows the multiplicity value up to which events are contained in the bin excluding all events contained in lower multiplicity bins.

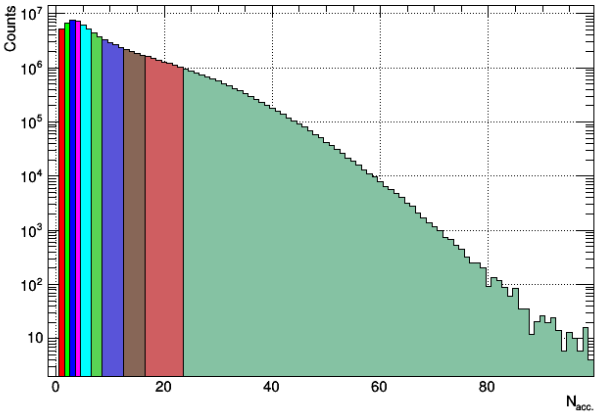

(a) CR, $|\eta| \leq 0.8$.

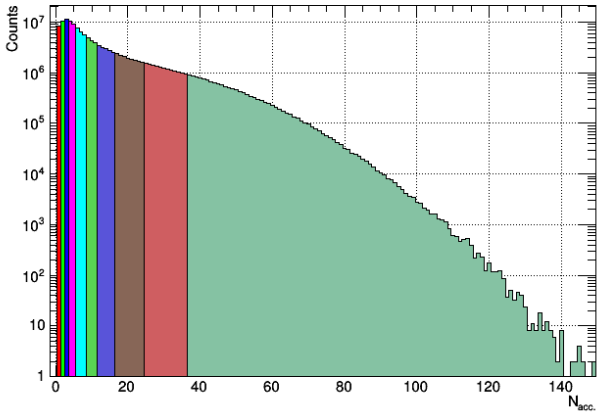

(b) No CR, $|\eta| \leq 0.8$.

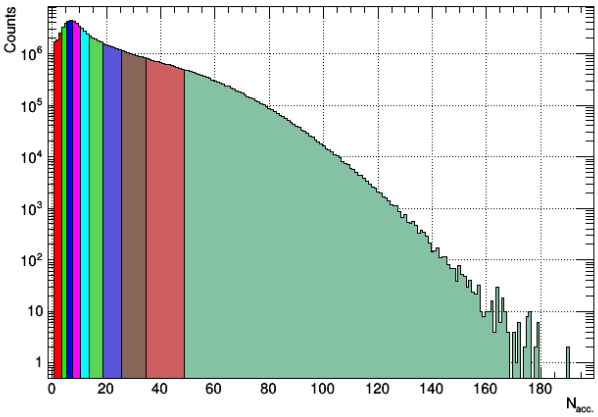

(c) CR, $|\eta| \leq 1.6$.

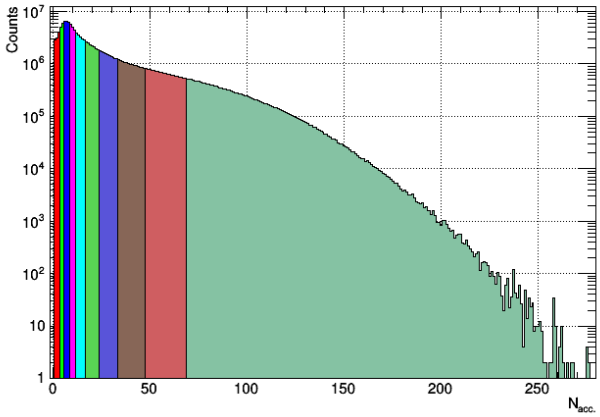

(d) No CR, $|\eta| \leq 1.6$.

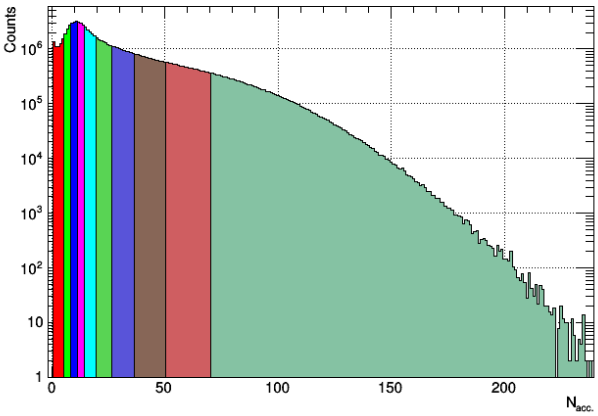

(e) CR, $|\eta| \leq 2.4$.

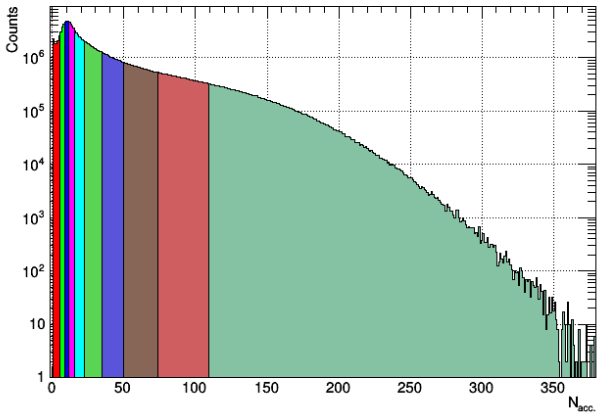

(f) No CR, $|\eta| \leq 2.4$.

Fig. 3: Multiplicity bins for the η ranges used in this analysis. Each colour represents a different multiplicity bin.

The events in the dataset without colour reconnection clearly show a higher mean multiplicity. With the exclusion of colour reconnection the mean multiplicity in the $|\eta| \leq 0.8$ range increases from 11 to 15. Similarly in $|\eta| \leq 1.6$ the mean multiplicity increases from 21 to 29. In $|\eta| \leq 2.4$ the mean multiplicity increases from 32 to 43.

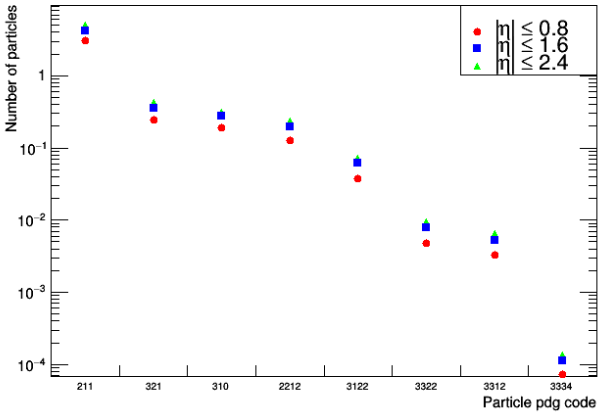

(a) Bin 10, CR.

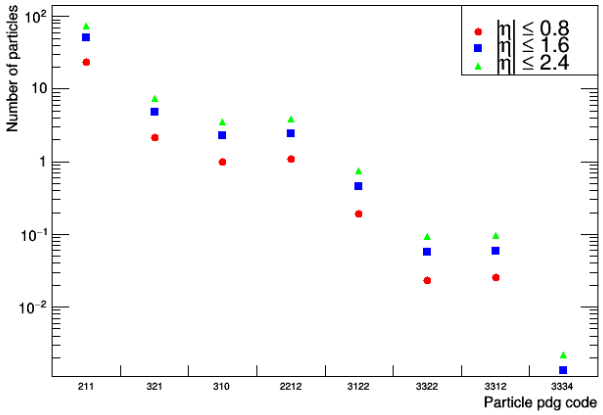

(b) Bin 1, CR.

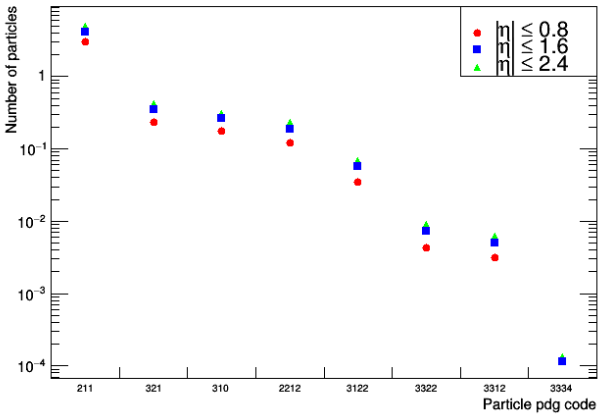

(c) Bin 10, No CR.

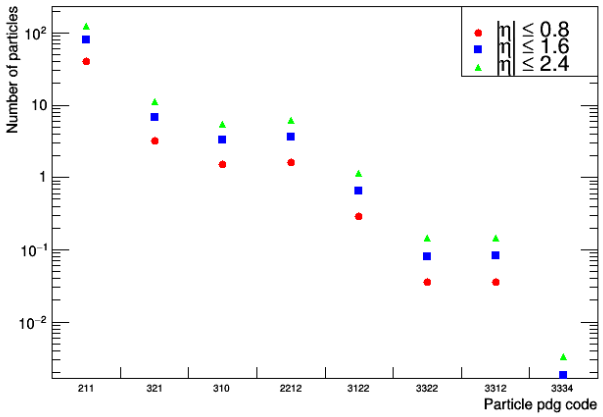

(d) Bin 1, No CR.

Fig. 4: The number of particles contained per multiplicity bin for specific particle species.

For the particle species that are used in this analysis we plotted the number of particles contained in the multiplicity bins. Figure 4 shows these plots for multiplicity bins 1 and 10, both for the CR and No CR dataset. These plots show that the number of particles contained in the bin drops off as the particle species mass increases, with bigger η range containing more particles. The number of particles contained grows for higher multiplicity bins. This is because the number of events per bin stays roughly equal while the mean multiplicity per event grows. The plot also shows that the number of particles contained in the bins for the No CR dataset are higher as we would expect given the fact that this dataset has a higher mean multiplicity overall.

7 Transverse momentum spectra

We plotted the transverse momentum (p_T) spectra for specific particle species contained in the various multiplicity bins. We normalized these spectra to the number of events for each multiplicity bin. Figure 7 shows these plots for multiplicity bins 1 and 10 for $|\eta| \leq 0.8$.

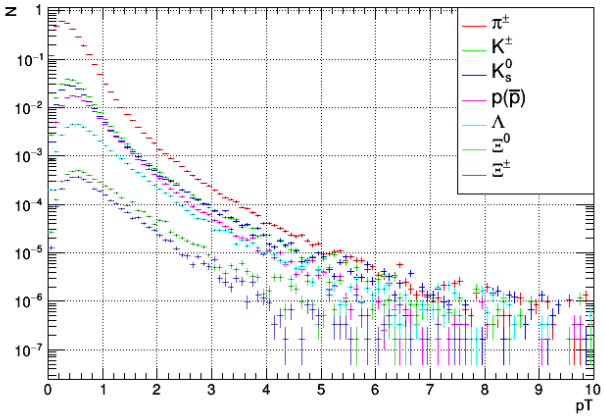

(a) Bin 10, CR, $|\eta| \leq 0.8$.

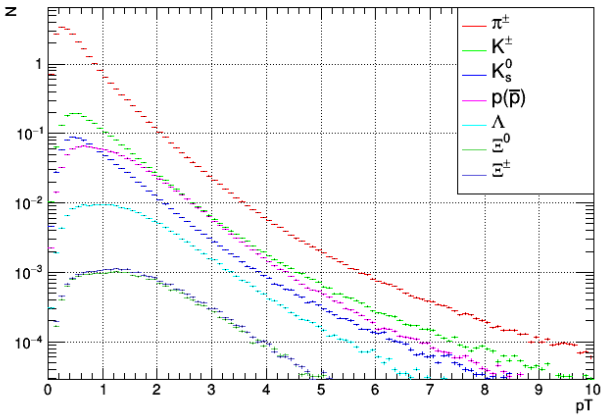

(b) Bin 1, CR, $|\eta| \leq 0.8$.

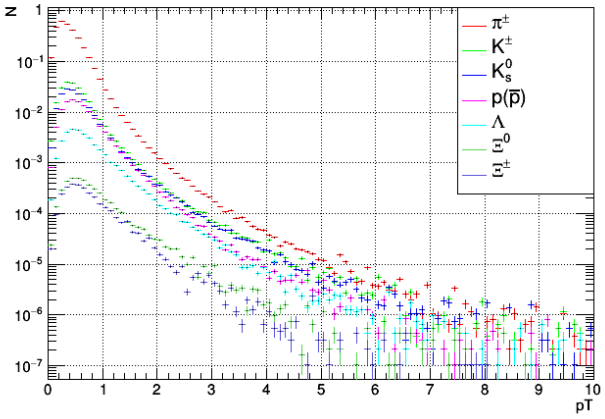

(c) Bin 10, No CR, $|\eta| \leq 0.8$.

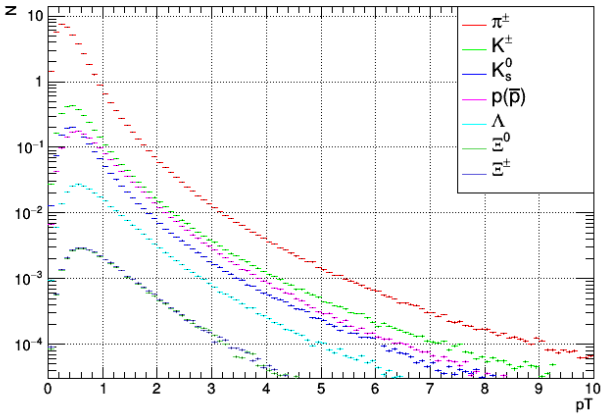

(d) Bin 1, No CR, $|\eta| \leq 0.8$.

Fig. 5: p_T spectra for specific particle species normalized to the number of events per bin in $|\eta| \leq 0.8$.

We can clearly see the particles with lower mass are dominant in the p_T spectrum. Bin 10 with CR (a) and bin 10 without CR (c) look very similar. Bin 1 with CR (b) and bin 1 without CR (d) however do show difference. The spectra look largely similar for lighter particles. For heavier particles the p_T spectrum shows a different slope. For the No CR case the slope is convex for higher p_T values and is very similar to the slopes in bin 1. In the case with CR however the p_T spectrum of heavier particles is concave and the spectrum as a whole looks more biased towards high p_T.

The η ranges $|\eta| \leq 1.6$ and $|\eta| \leq 2.4$ are similarly plotted in figure 6. They show the same behaviour as we see in $|\eta| \leq 0.8$.

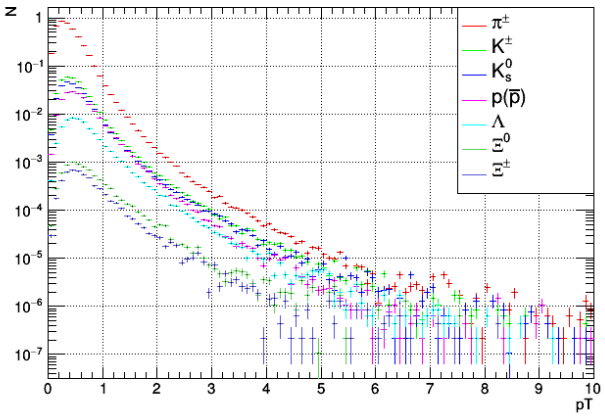

(a) Bin 10, CR, $|\eta| \leq 1.6$.

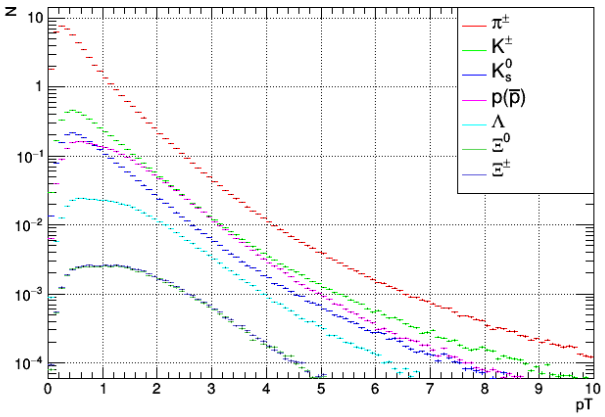

(b) Bin 1, CR, $|\eta| \leq 1.6$.

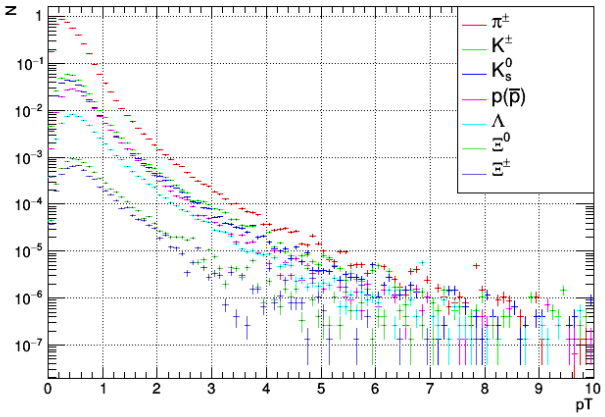

(c) Bin 10, No CR, $|\eta| \leq 1.6$.

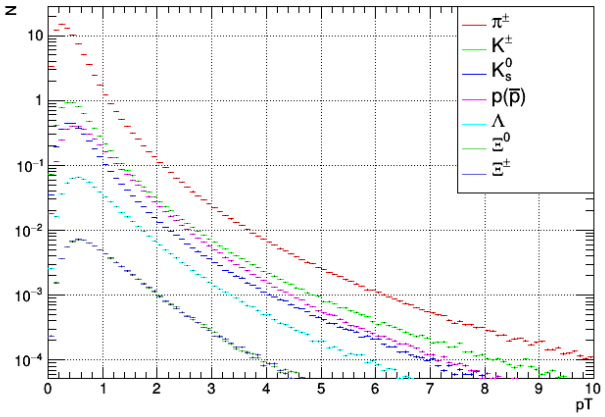

(d) Bin 1, No CR, $|\eta| \leq 1.6$.

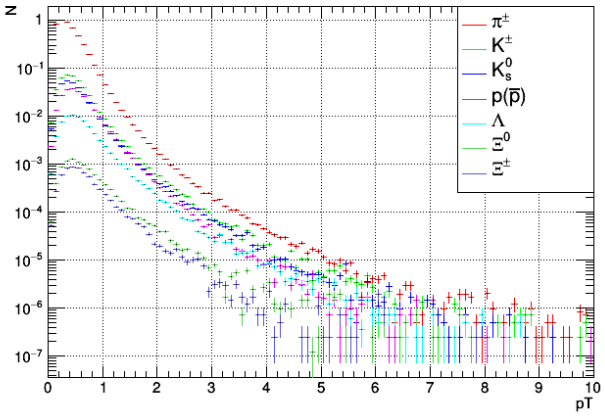

(e) Bin 10, CR, $|\eta| \leq 2.4$.

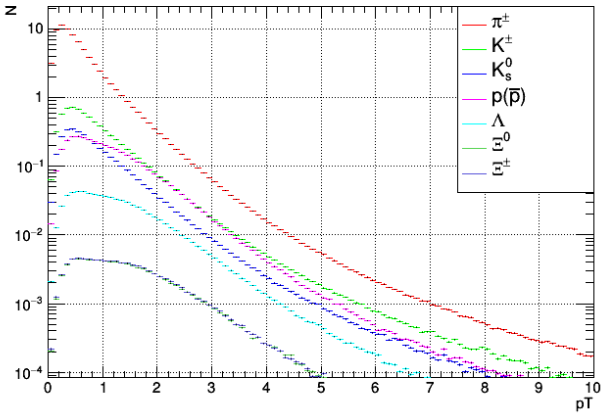

(f) Bin 1, CR, $|\eta| \leq 2.4$.

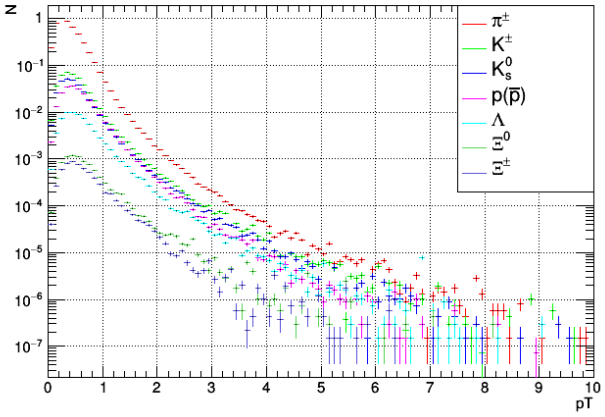

(g) Bin 10, No CR, $|\eta| \leq 2.4$.

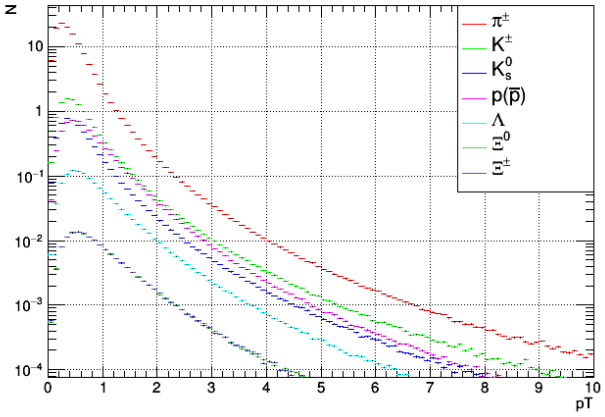

(h) Bin 1, No CR, $|\eta| \leq 2.4$.

Fig. 6: p_{T} spectra for specific particle species normalized to the number of events per bin for $|\eta| \leq 1.6$ and $|\eta| \leq 2.4$.

For the p_T behaviour of specific particle species it is more interesting to normalize the particle species p_T spectrum to the number of particles of this species contained in the multiplicity bin. This sets the integral over the p_T spectrum for all particle species to unity. When the integral of all particle species spectra is equal we can compare their shape and make qualitative statements about their behaviour relative to each other. Figure 7 shows these spectra both for CR and no CR in $|\eta| \leq 0.8$.

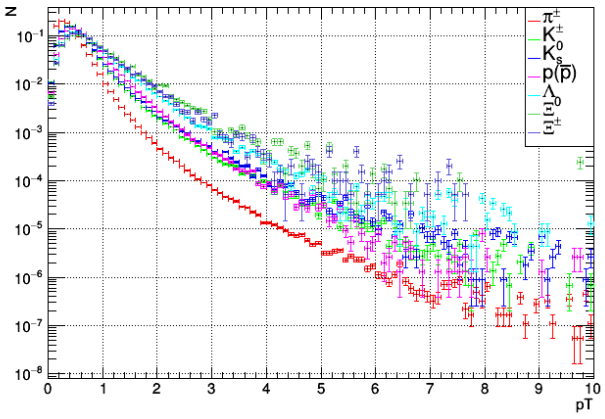

(a) Bin 10, CR, $|\eta| \leq 0.8$.

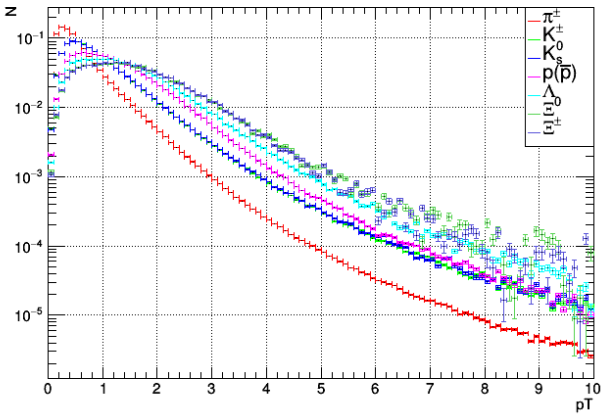

(b) Bin 1, CR, $|\eta| \leq 0.8$.

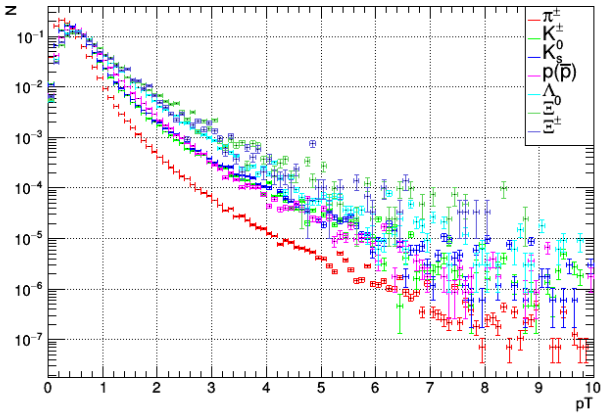

(c) Bin 10, No CR, $|\eta| \leq 0.8$.

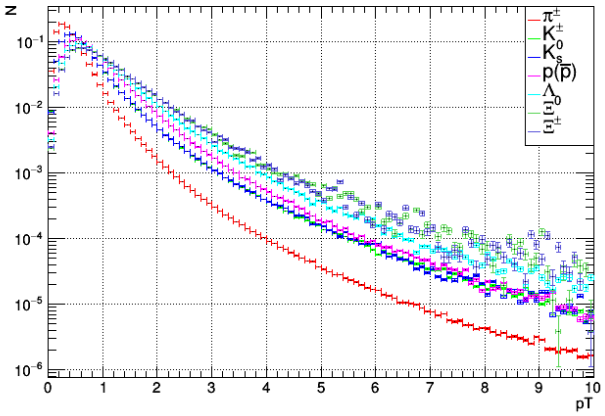

(d) Bin 1, No CR, $|\eta| \leq 0.8$.

Fig. 7: p_T spectrum for specific particle species in $|\eta| \leq 0.8$. All spectra normalized to the same integral.

We can now clearly see that in the CR dataset the heavier particles undergo a 'boost' in p_T for higher multiplicity while in the no CR case there is not such an effect. The p_T spectrum changes from convex to concave for higher values op p_T. It seems this effect is mass dependent as heavier particles see a clearer change is shape while the lightest particles show no clear difference to the low multiplicity case. Figure 8 shows these same plots for $|\eta| \leq 1.6$ and $|\eta| \leq 2.4$.

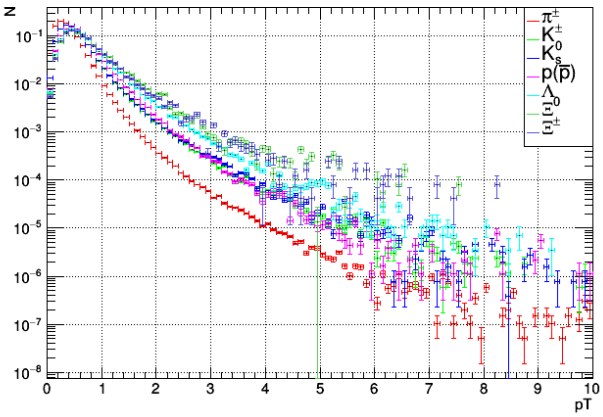

(a) Bin 10, CR, $|\eta| \leq 1.6$.

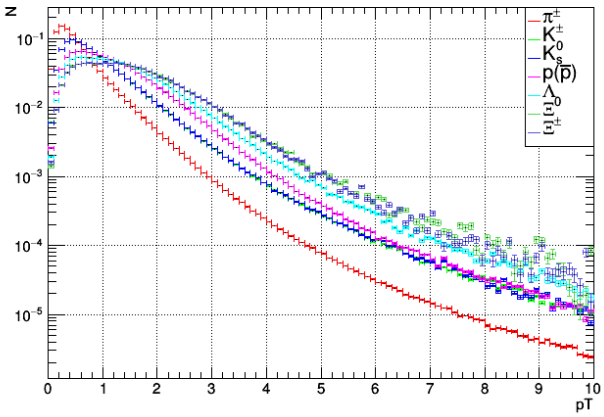

(b) Bin 1, CR, $|\eta| \leq 1.6$.

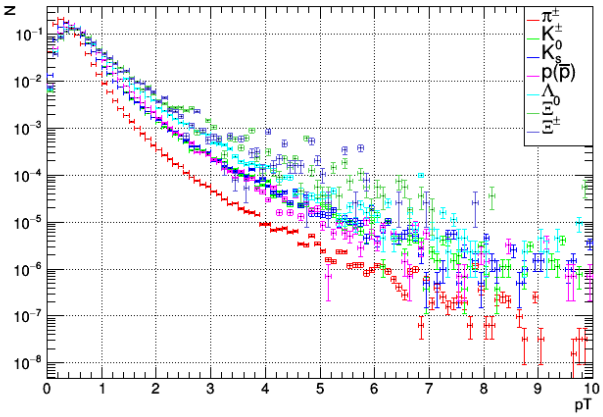

(c) Bin 10, No CR, $|\eta| \leq 1.6$.

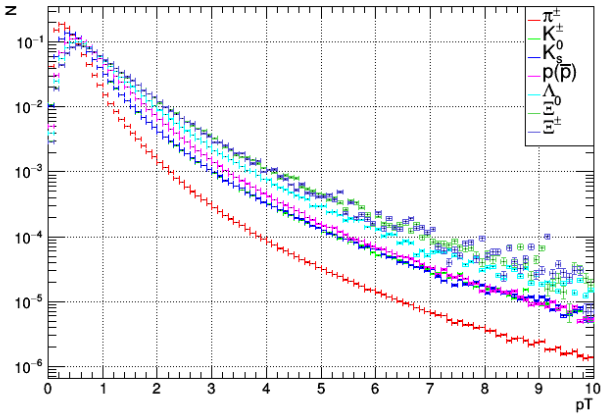

(d) Bin 1, No CR, $|\eta| \leq 1.6$.

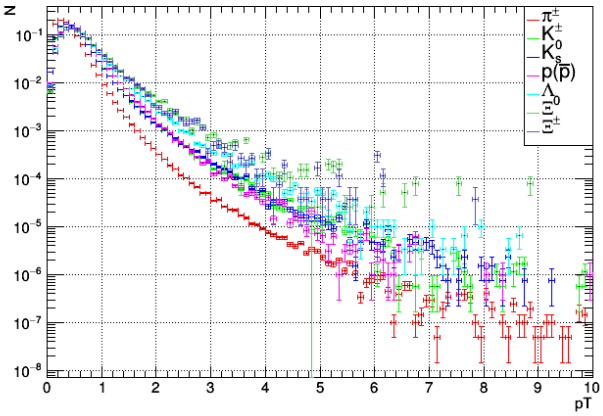

(e) Bin 10, CR, $|\eta| \leq 2.4$.

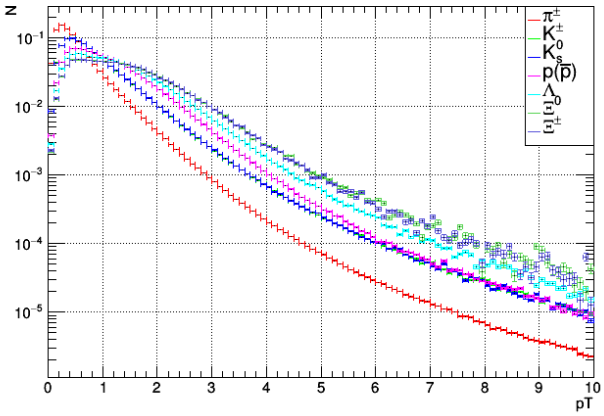

(f) Bin 1, CR, $|\eta| \leq 2.4$.

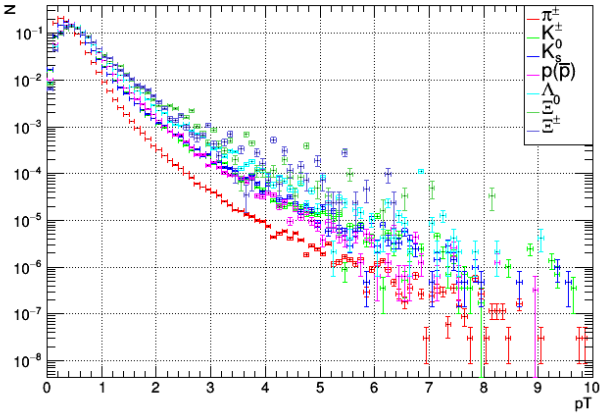

(g) Bin 10, No CR, $|\eta| \leq 2.4$.

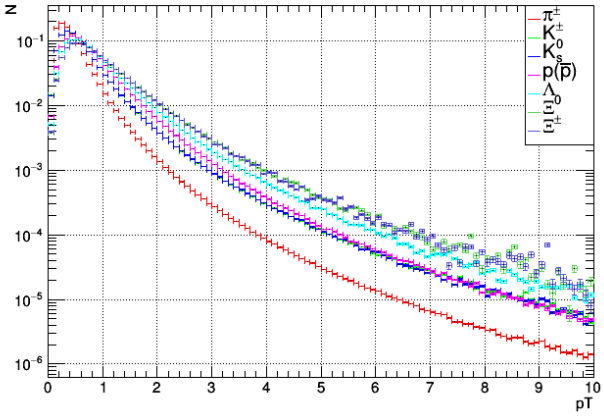

(h) Bin 1, No CR, $|\eta| \leq 2.4$.

Fig. 8: p_{T} spectrum for specific particle species in $|\eta| \leq 1.6$ and $|\eta| \leq 2.4$. All spectra normalized to the same integral.

8 Particle dependent mean transverse momentum

Out of the p_T spectra of the particle species we can extract a mean for the value of p_T over all multiplicity bins. We have plotted these values for mean p_T in figure 9. The particles in the dataset with CR have an overall higher mean p_T. In both CR and no CR datasets the heavier particles have a higher mean p_T. The plots for the dataset with colour reconnection show a clear increase in mean p_T over the no CR case which seems most significant for heavy particles.

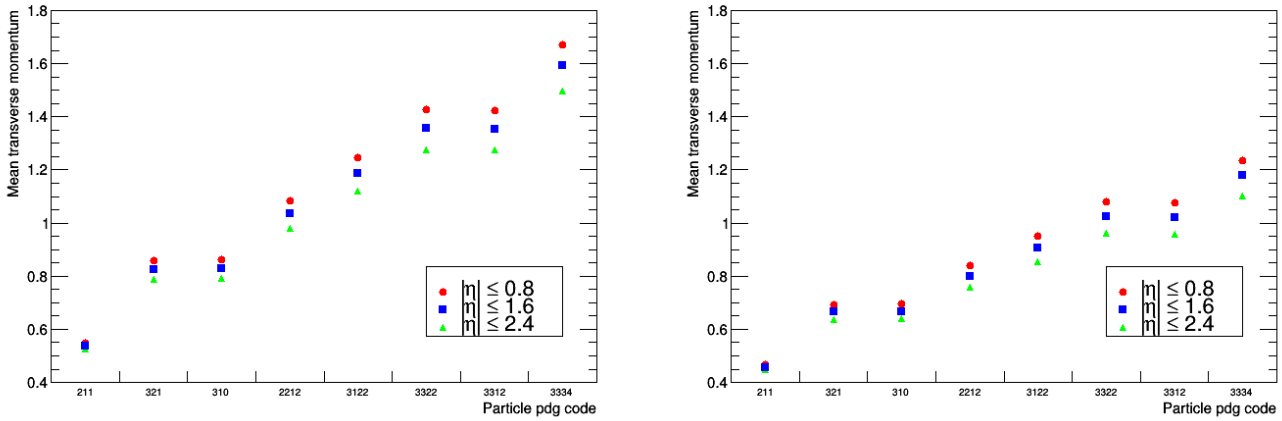

(a) CR, $|\eta| \leq 2.4$. (b) No CR, $|\eta| \leq 2.4$.

Fig. 9: Mean value of p_T over all multiplicity bins.

We have also plotted the mean p_T value for the individual multiplicity bins. This plot for $|\eta| \leq 0.8$ can be seen in figure 10. The plots for the dataset with colour reconnection show a clear increase in mean p_T for more massive particles, as well as a clear increase in mean p_T for increasing multiplicity. The no CR plots shows an increase in mean p_T for heavier particles. The increase for multiplicity seen in the no CR case is much less pronounced compared to the CR case.

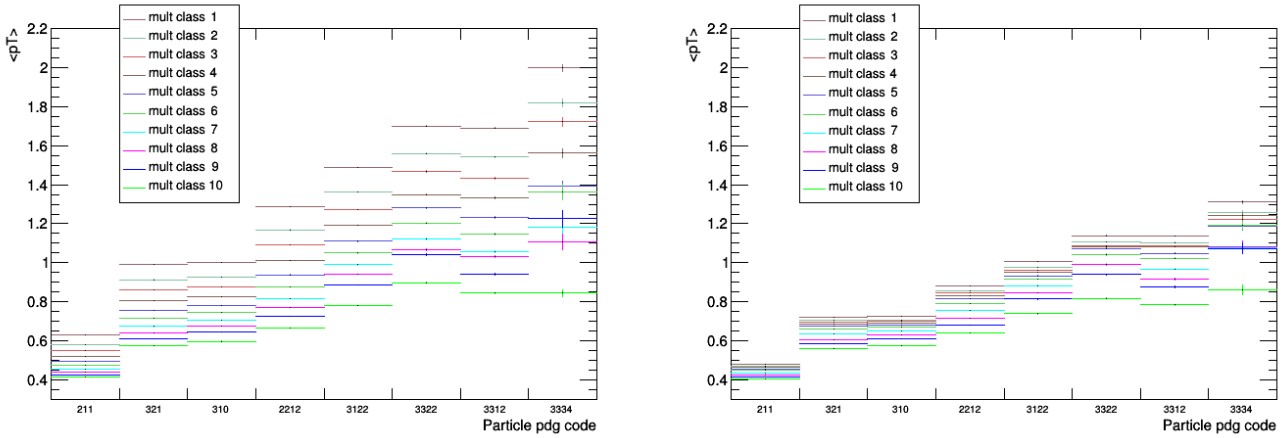

(a) CR, $|\eta| \leq 0.8$. (b) No CR, $|\eta| \leq 0.8$.

Fig. 10: Mean p_T for particle species in multiplicity bins.

The same plot for $|\eta| \leq 1.6$ and $|\eta| \leq 2.4$ can be found in figure 11. These plots show very similar behaviour to the $|\eta| \leq 0.8$ case. The main difference they exhibit is an overall lower mean p_T. This is easily explained by figure 9 which indeed shows that larger η ranges have a lower overall mean p_T.

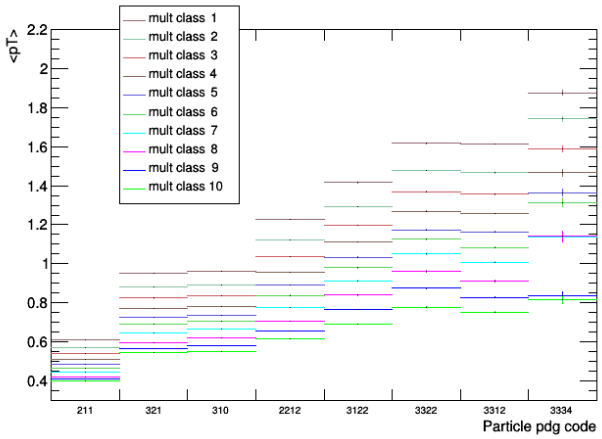

(a) CR, $|\eta| \leq 1.6$.

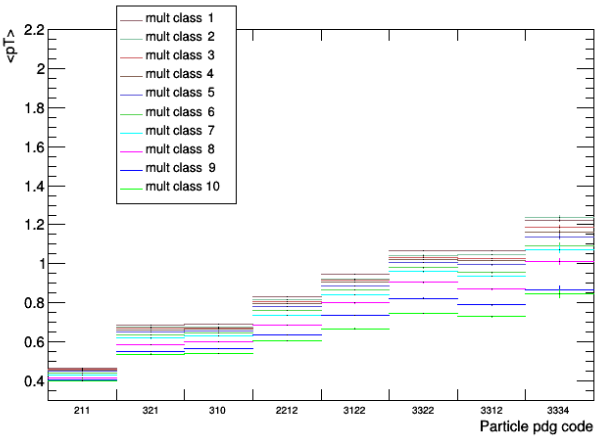

(b) No CR, $|\eta| \leq 1.6$.

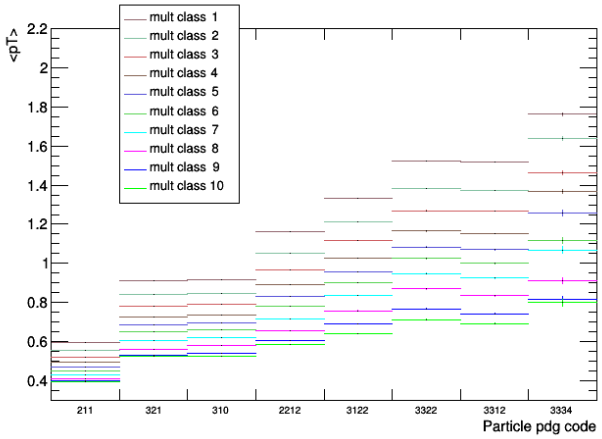

(c) CR, $|\eta| \leq 2.4$.

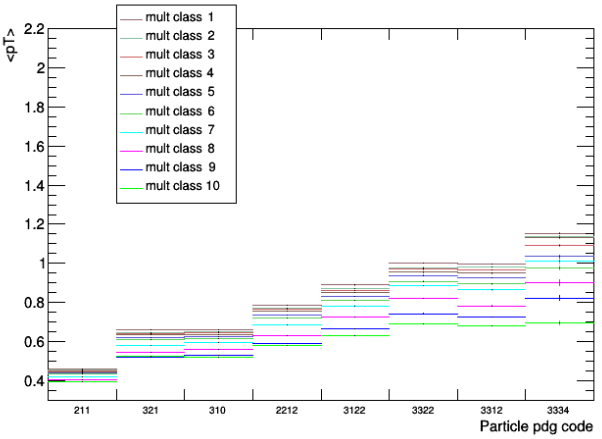

(d) No CR, $|\eta| \leq 2.4$.

Fig. 11: Mean p_{T} for particle species in multiplicity bins.

In order to study the particle and multiplicity dependence of the mean p_{T} we plotted the ratio between the mean p_{T} values shown in figure 10 and figure 11 and the mean p_{T} over all multiplicity bins for the specific particles shown in figure 9. These ratios are shown in figure 12.

The ratios show a significantly wider range for the CR dataset. This indicates that the CR mechanism does play a big role in the p_{T} distribution. The heavier the particle the more spread out the ratios become, however for the lighter particles the ratios still differ significantly from the no CR case. This suggest the CR mechanics also plays a role in the p_{T} spectrum for lighter particles.

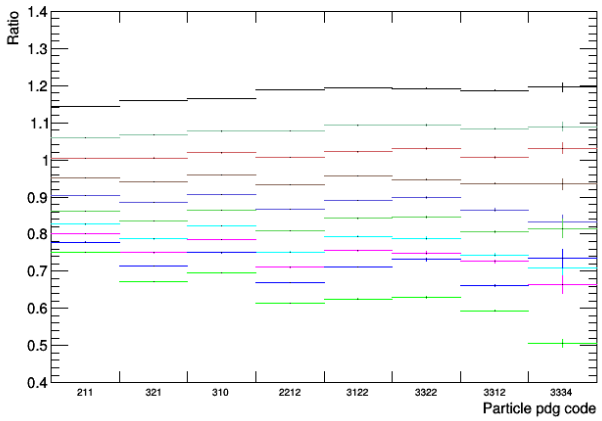

(a) CR, $|\eta| \leq 0.8$.

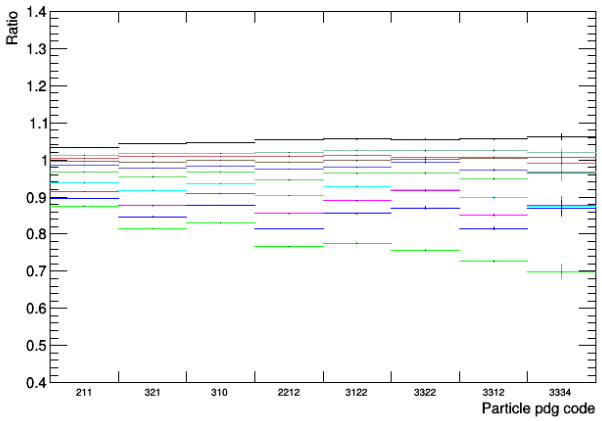

(b) No CR, $|\eta| \leq 0.8$.

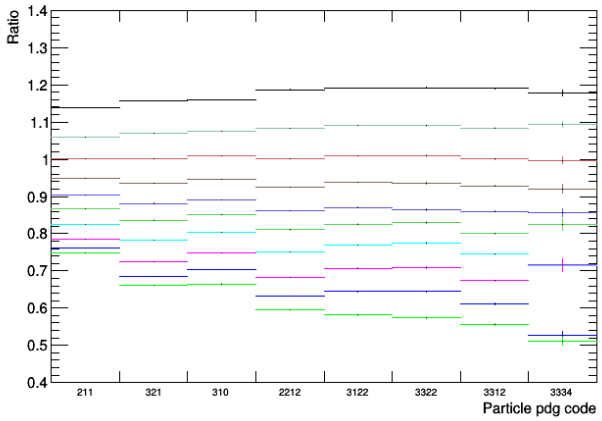

(c) CR, $|\eta| \leq 1.6$.

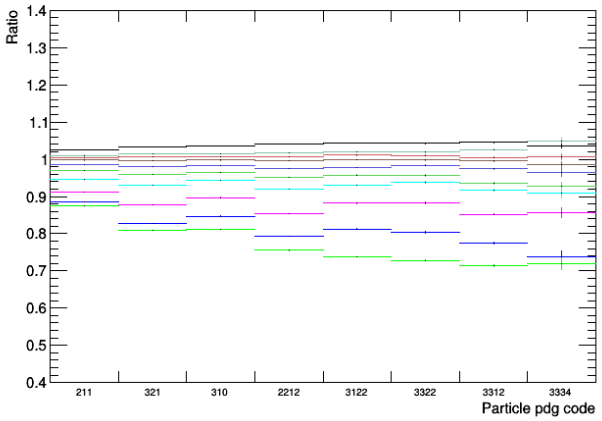

(d) No CR, $|\eta| \leq 1.6$.

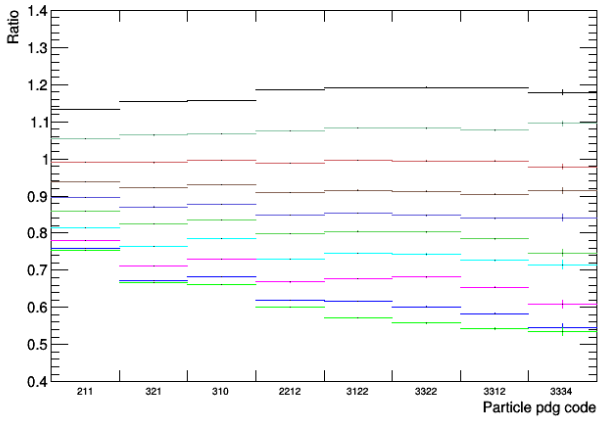

(e) CR, $|\eta| \leq 2.4$.

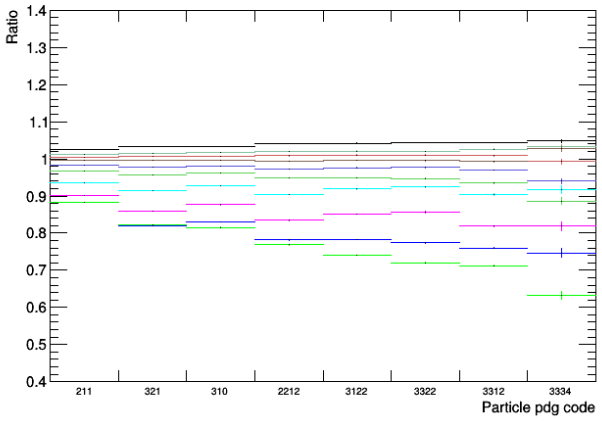

(f) No CR, $|\eta| \leq 2.4$.

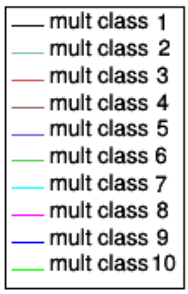

(g) Legend for figures a-f

Fig. 12: Ratio between mean p_{T} for specific bins and mean p_{T} over all bins.

9 Mass dependent mean transverse momentum

The previous figures showed that the CR mechanism seemed to have a stronger effect on more massive particles. With the mean transverse momentum being up to 60% higher for high multiplicity events compared to the no CR case. For the low multiplicity events the mean transverse momentum stayed roughly equivalent. In order to better understand this mass dependence of the CR mechanism we redid some of the previous calculations for particle mass instead of particle species using table 1. The mean transverse momentum for all multiplicity bins for particle mass can be seen in figure 13. When the mean transverse momentum is plotted against particle mass it roughly seems to behave linearly. We also redid the ratio between mean transverse momentum per multiplicity bin and mean transverse momentum over all multiplicity bins in figure 14. This figure shows us that the mass dependence of the CR mechanism is much more significant for low multiplicity events, with the heaviest particle being affected roughly twice as much as the lightest particle. For the high multiplicity events this difference between light and heavy particles is smaller. The difference in effect between the lightest and heaviest particle in high multiplicity is below ten percent.

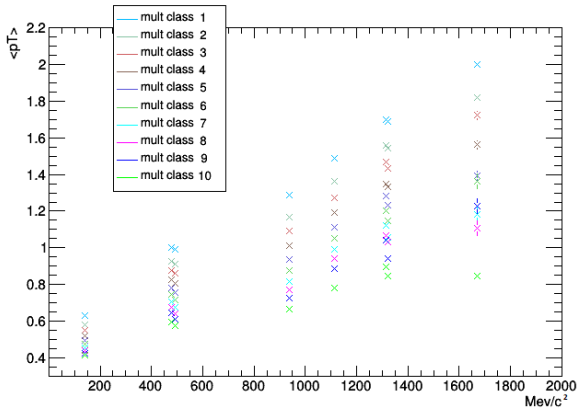

(a) CR, $|\eta| \leq 0.8$.

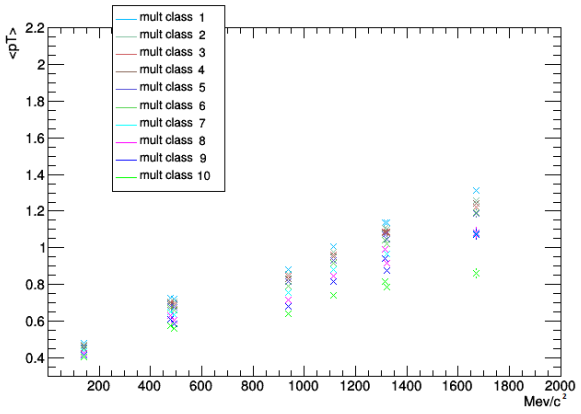

(b) No CR, $|\eta| \leq 0.8$.

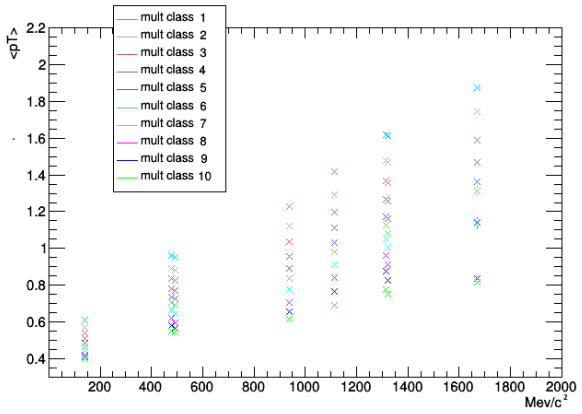

(c) CR, $|\eta| \leq 1.6$.

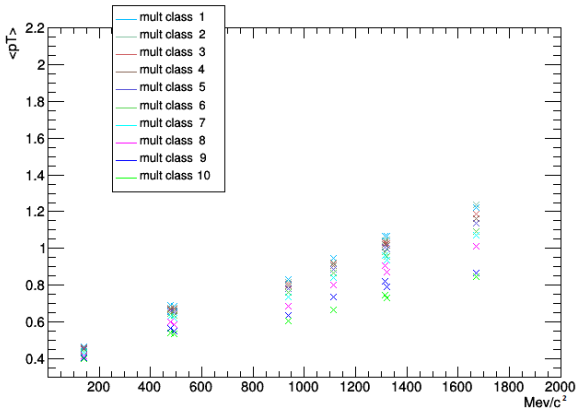

(d) No CR, $|\eta| \leq 1.6$.

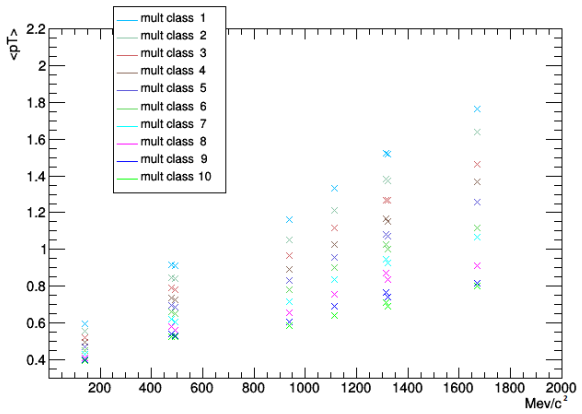

(e) CR, $|\eta| \leq 2.4$.

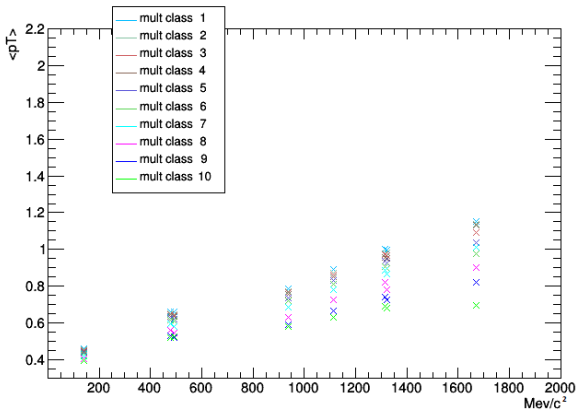

(f) No CR, $|\eta| \leq 2.4$.

Fig. 13: Mean p_{T} for particle mass in multiplicity bins.

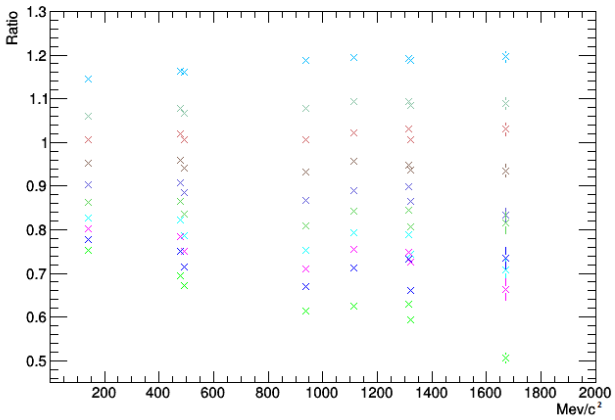

(a) CR, $|\eta| \leq 0.8$.

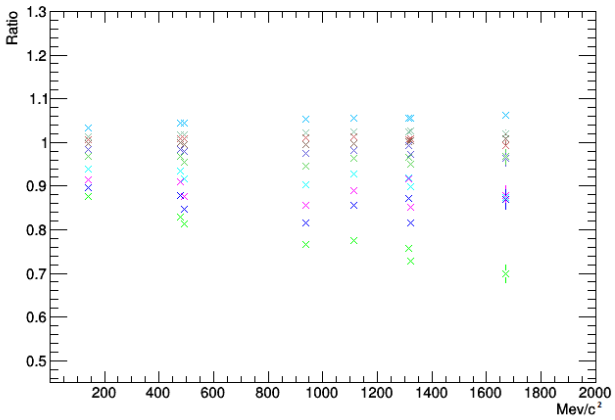

(b) No CR, $|\eta| \leq 0.8$.

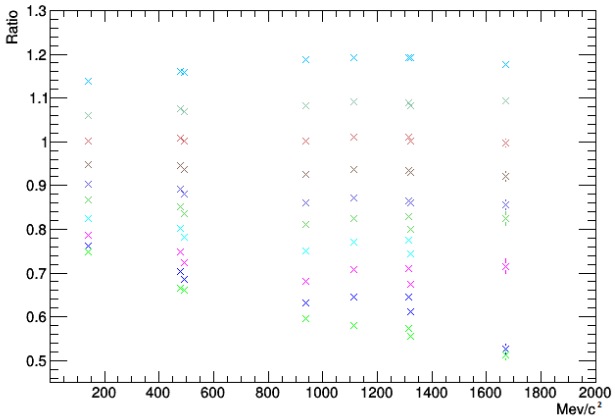

(c) CR, $|\eta| \leq 1.6$.

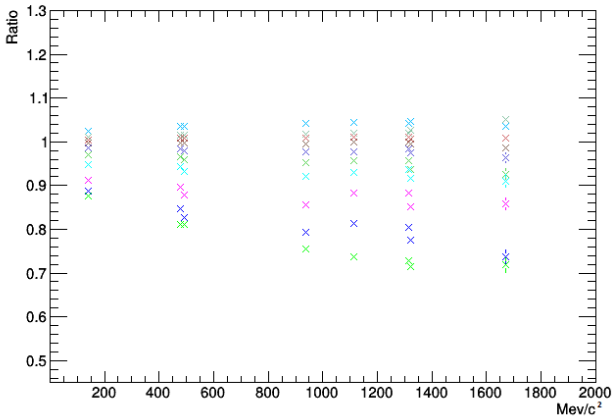

(d) No CR, $|\eta| \leq 1.6$.

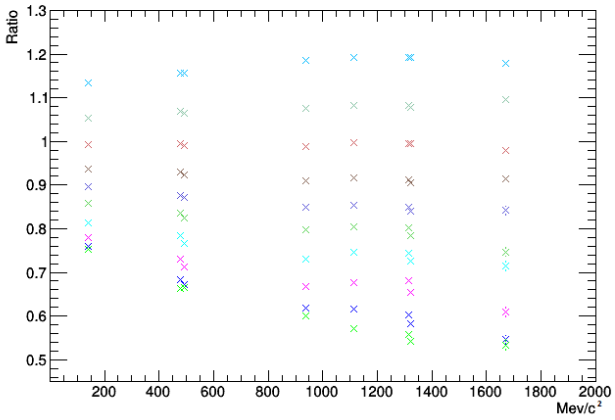

(e) CR, $|\eta| \leq 2.4$.

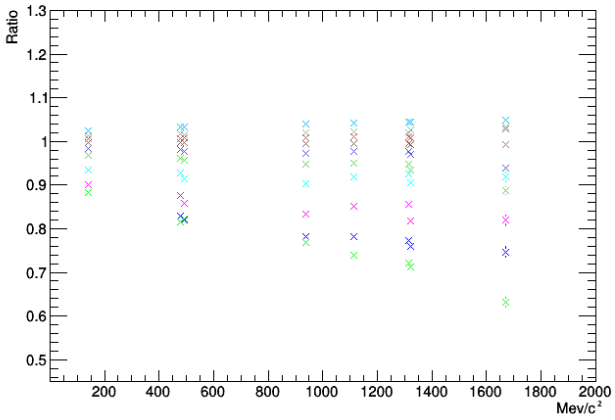

(f) No CR, $|\eta| \leq 2.4$.

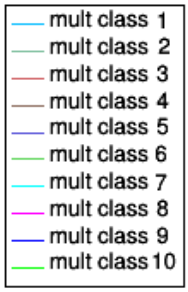

(g) Legend for figures a-f

Fig. 14: Mean p_{T} for particle mass in multiplicity bins.

Part V. Results

The main results of this thesis is a quantitative comparison between mean transverse momentum for CR and no CR events. These results can be found in figure 15. They show the ratio between the mean transverse momentum for CR and no CR events for all multiplicity bins both for particle species and particle mass. The lowest ratio values represent the highest multiplicity bins with the ratio rising for every lower multiplicity bin. The data shows that for the highest 4 multiplicity bins, bins 10, 9, 8 and 7, the CR dataset has a slightly lower average mean transverse momentum in comparison to the no CR dataset, while the lower multiplicity bins have a significant higher mean transverse momentum over the no CR dataset.

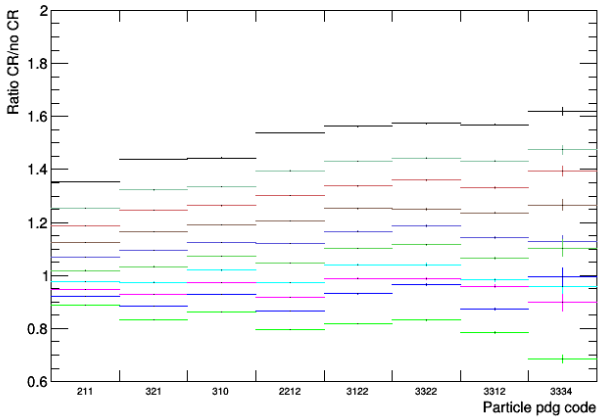

(a) $|\eta| \leq 0.8$.

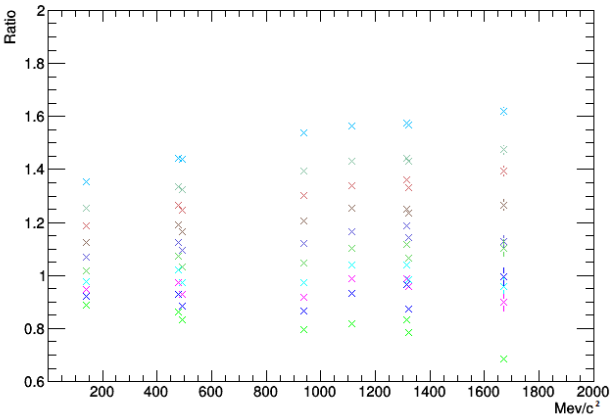

(b) $|\eta| \leq 0.8$.

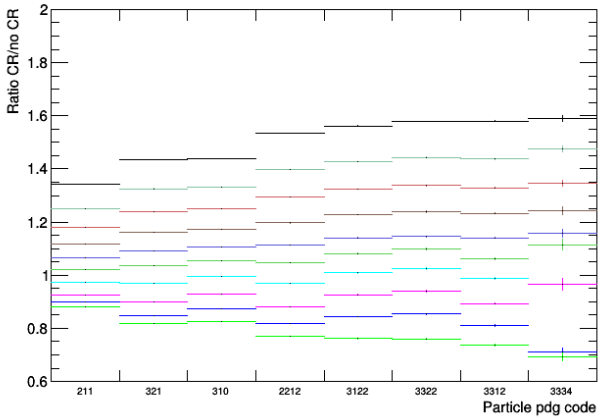

(c) $|\eta| \leq 1.6$.

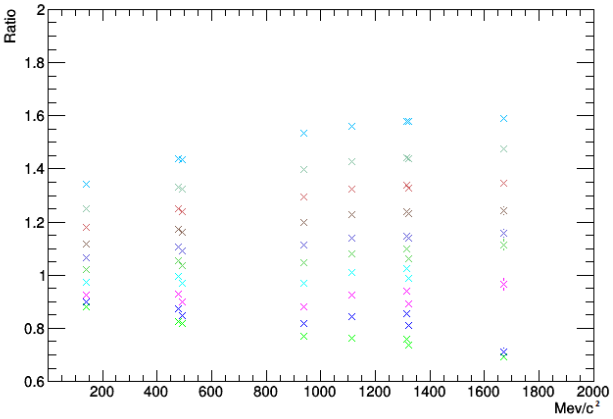

(d) $|\eta| \leq 1.6$.

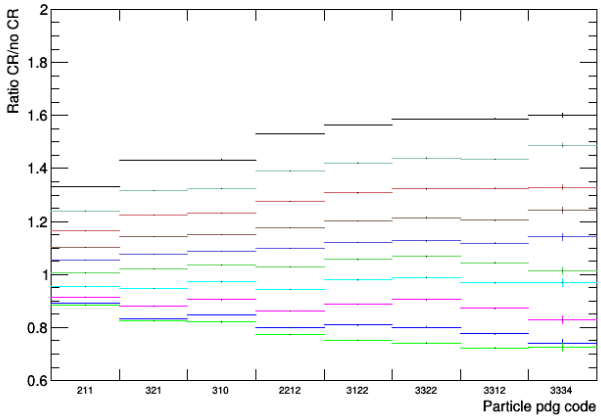

(e) $|\eta| \leq 2.4$.

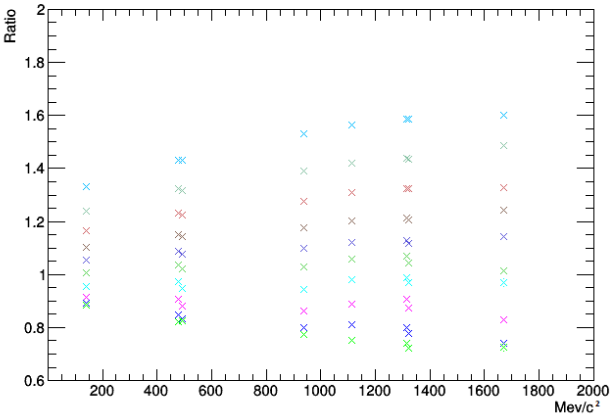

(f) $|\eta| \leq 2.4$.

Fig. 15: Ratio of mean transverse momentum ratio for CR against no CR for individual multiplicity bins.

Part VI. Discussion and conclusion

Our results show a clear influence of the colour reconnection mechanism on the transverse momentum spectra for pp events in PYTHIA. The overall mean transverse momentum for events with colour reconnection is significantly higher than for particles without colour reconnection. When we also take multiplicity into account we see that for low multiplicity events the mean transverse momentum for colour reconnection events is actually slightly lower in comparison to the non colour reconnected dataset. This effect is however overshadowed by the significant boost in transverse momentum for particles in high multiplicity events as can easily been seen in the left column of figure 15.

The effects of the colour reconnection mechanism on the transverse momentum seems to be more prominent in heavier particles. The right column of figure 15 seems to suggest a linear mass dependence for the increased transverse momentum. In order to be able to better quantify the mass dependence more particles could be added in further analysis. Particle yield however decreases with increased particle mass. This might provide difficulties with the analysis of exceedingly rare particle species.

The first noticeable difference between the colour reconnected and non colour reconnected dataset was the significantly higher multiplicity the non colour reconnected dataset boasted. This is however easily explained with the results of this analysis on the basis of energy conservation. Because the colour reconnected dataset has a higher mean transverse momentum for its particles less energy is available for particle creation.

In order to better understand the multiplicity dependence of the colour reconnection mechanism more multiplicity bins might be added in further analysis. In this analysis bins of 10% multiplicity were used. It is however possible to work with smaller bins like for example bins of 5%. This will be at the cost of bigger errors, which can be compensated by bigger datasets with more events. One might also go so far as to forgo the binning of multiplicity altogether. This will result in an average p_T spectrum with many more entries at the cost of bigger errors. This can however can also be compensated with bigger datasets.

Data published by the ALICE collaboration for mean transverse momentum against multiplicity for proton proton collisions show an increase of transverse momentum for high multiplicity as seen in figure 16. The physics behind this increase might be of the same nature as the increase in mean transverse momentum discussed in this paper, however, more research is needed to explain this phenomenon satisfactorily.

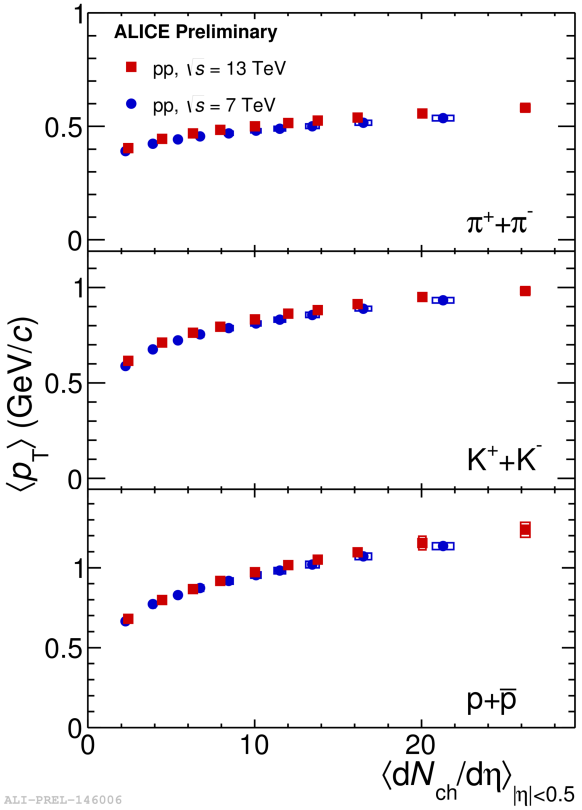

Fig. 16: Mean transverse momentum versus multiplicity from preliminary ALICE article [5].

Part VII. References

References

[1] T. Sjöstrand et al., An Introduction to PYTHIA 8.2, Comput. Phys. Commun. 191 (2015) 159, arXiv: 1410.3012 [hep-ph].

[2] "ALICE forges ahead with detector installation", CERN Courier. December 2006.

[3] Hisayuki Torii, Midrapidity Neutral-Pion Production in Proton-Proton Collisions at $\sqrt{s}$ = 200GeV. July 2004.

[4] C. Patrignani et al. (Particle Data Group), Chin. Phys. C, 40, 100001 (2016) and 2017 update

[5] ALICE preliminary result 146006 as presented by Ajay Kumar Dash. Retrieved from https://indico.cern.ch/event/656452/contributions/2869642/attachments/1648338/2635232/AKDashQM2018Final.pdf